

Relativistic theoretical description for spin-resolved *CVV* Auger electron spectroscopy with application to Pd and Fe

J. Minár, V. Popescu, and H. Ebert

Physikalische Chemie, Universität München, Butenandtstrasse 5-13, D-81377 Munich, Germany

(Received 12 April 2000)

A theoretical description of spin-resolved *CVV* (core-valence-valence) Auger electron spectroscopy is presented. The approach is derived on the basis of a fully relativistic description of the electronic structure of magnetic materials. As a consequence, spontaneous exchange splitting as well as spin-orbit coupling—two possible and important sources for a spin-polarization of Auger electrons—are accounted for on the same level. This is demonstrated by application to paramagnetic fcc Pd and ferromagnetic bcc Fe. In both cases spin-resolved *CVV* Auger electron spectra are presented and discussed emphasizing the role of the spin-orbit coupling. Comparison is made with available experimental data as far as possible.

I. INTRODUCTION

Spectroscopies involving tightly bound core states, as for example x-ray absorption and emission, Auger-electron spectroscopy, or resonant photoemission, are nowadays standard tools to probe the electronic structure of transition-metal systems in an element-specific way. Recently, many experiments focused on the local magnetic properties of ferromagnets, antiferromagnets, and so on by exploiting the magnetic circular dichroism and/or spin analysis for outgoing electrons.^{1,2} By investigating the core-valence-valence (*CVV*) Auger-electron spectroscopy (AES) of Fe in pure Fe and other magnetic materials Landolt and co-workers could demonstrate that for magnetically ordered solids the spin polarization of the Auger electrons is a direct consequence of the spin polarization of the valence-band electrons.^{3,4} The experiments of these authors were performed by using unpolarized electrons for the excitation step. Using circularly polarized radiation instead leads to spin-polarized *CVV* Auger electrons even for paramagnetic solids as shown by Stoppmanns *et al.*, for example, for K.⁵ Here the spin polarization of the Auger electrons has to be ascribed to a preferential depopulation of the core levels in the $M_{2,3}$ shell during the excitation step that differ in their magnetic quantum number μ . Recently, linearly and circularly polarized radiation has been used also for spin-resolved *CVV* AES investigations on magnetically ordered systems.^{6,7} Of course this leads to a more complex situation because now spin polarization of the Auger electrons may be caused simultaneously by the two aforementioned mechanisms.

In the following a theoretical approach is presented that is meant to supply a rather general description for *CVV* AES and allows in particular a discussion of the various experiments mentioned above. Concerning the theoretical description of AES for transition-metal systems two main streams can be identified. On the one hand many approaches are primarily meant to account properly for correlation, i.e., many-body effects.^{8–10} For that reason the underlying electronic band structure of the investigated system is in general represented in a simplified way using appropriate models. On the other hand, one may more or less ignore many-body

effects and put more effort in the treatment of the electronic band structure.^{11,12} Adopting the latter approach one is immediately led to the standard interpretation of *CVV* AES spectra in terms of a self-convolution of the density of states (DOS) for the states below the Fermi level.¹³ This point of view proved to be astonishingly successful in the past even for the spin-resolved case as it was demonstrated, for example, by Sinković *et al.* who studied the $L_{2,3}VV$ spectra of S for the system $c(2 \times 2)S/Fe(001)$.^{14,15} This experience is also in line with the recent experimental and theoretical work on spin-resolved appearance potential spectroscopy (APS) that can be seen as an inverse *CVV* AES experiment.^{16,17} These investigations in particular demonstrated the importance of the Coulomb matrix elements that for $L_{2,3}VV$ spectra transition-metal systems strongly favor transitions involving the d electrons of the valence band.

The occurrence of spin-polarized Auger electrons for paramagnetic solids when circularly polarized radiation is used for the excitation step can be traced back to the presence of spin-orbit coupling. For magnetically ordered systems this leads to a rather complex situation. For that reason it seems to be appropriate to start from a single-particle picture, i.e., to adopt the second theoretical approach and to add many-body corrections later if necessary. This route has been followed here by generalizing the relativistic theoretical description of *CVV* AES worked out by Szunyogh *et al.*¹¹ to allow application to spin-polarized systems as well. The formalism is presented in short in the next section. A number of applications will be presented in the following sections together with a detailed discussion.

II. THEORETICAL APPROACH AND TECHNICAL DETAILS

As mentioned above, our theoretical approach to deal with the *CVV* AES of magnetic solids is essentially a generalization of the scheme developed by Szunyogh *et al.*¹¹ to deal with paramagnetic solids. For that reason only the most important steps are given here.

Starting point is the standard expression for the Auger

process transition probability¹⁸

$$I \propto \sum_{\alpha_A, \alpha_B, \alpha_C, \alpha_D} |D-E|^2 \delta(E_B - E_A + E_D - E_C). \quad (1)$$

Here D and E are the so-called direct and exchange Coulomb matrix elements for the various involved single-particle states ψ_i . These states have energy E_i and are labeled by appropriate quantum numbers α_i . For the CVV AES case, ψ_{α_B} and ψ_{α_C} are initially occupied valence-band states, while ψ_{α_A} is an initially unoccupied core state. Finally, ψ_{α_D} is the state representing the outgoing Auger electron.

To evaluate the matrix elements occurring in Eq. (1) the Coulomb interaction operator is represented by the following expansion:

$$\frac{1}{|\vec{r}_1 - \vec{r}_2|} = \sum_{\lambda\mu} \frac{4\pi}{2\lambda+1} \frac{r_{<}^\lambda}{r_{>}^{\lambda+1}} Y_{\lambda\mu}(\hat{r}_1) Y_{\lambda\mu}^*(\hat{r}_2). \quad (2)$$

Adopting a relativistic formulation, the core states wave function ψ_{Λ_A} is given by

$$\psi_{\Lambda_A}(\vec{r}, E) = \sum_{\Lambda'} \begin{pmatrix} g_{\Lambda' \Lambda_A}(r, E) \chi_{\Lambda'}(\hat{r}) \\ i f_{\Lambda' \Lambda_A}(r, E) \chi_{-\Lambda'}(\hat{r}) \end{pmatrix} \quad (3)$$

and is obtained as a solution of the Dirac equation.¹⁹ Dealing with the magnetically ordered state of a solid within the framework of SDFT (spin density-functional theory) this equation contains a spin-dependent potential term.²⁰ As a consequence, the functions ψ_{Λ_A} will in general have no unique spin-angular character $\Lambda_A = (\kappa, \mu)$ (κ and μ are the relativistic spin-orbit and magnetic quantum numbers²¹) but one has a superposition of contributions with character Λ' . Replacing $|D-E|^2$ in Eq. (1) by $(D-E)(D-E)^*$ the valence-band states ψ_{α_B} and ψ_{α_C} always occur in the form

$$\sum_{\alpha_C} \psi_C(\vec{r}) \psi_C^\dagger(\vec{r}') \delta(E - E_C). \quad (4)$$

For a periodic bulk system one could represent the functions ψ_C by Bloch-type wave functions. A more general formalism is achieved replacing the expression given above by

$$\frac{1}{2\pi i} [G^+(\vec{r}, \vec{r}', E) - G^-(\vec{r}, \vec{r}', E)], \quad (5)$$

where $G^+(\vec{r}, \vec{r}', E)$ and $G^-(\vec{r}, \vec{r}', E)$ are the retarded and advanced Green's functions, respectively. Using spin-polarized relativistic multiple-scattering theory they can be written for most situations as^{22,23}

$$\sum_{\Lambda \Lambda'} Z_{\Lambda}^n(\vec{r}, E) \mathfrak{T}_{\Lambda \Lambda'}^{nn}(E) Z_{\Lambda'}^{n \times}(\vec{r}', E). \quad (6)$$

Here the wave functions Z_{Λ}^n are the regular solutions at energy E to the Dirac equation for a spin-dependent potential at lattice site n . As for the core states, the functions Z_{Λ}^n will in general have no unique spin-angular character. The quantity $\tau_{\Lambda \Lambda'}^{nn}$, used in the above expression is the so-called scattering path operator that describes all multiple-scattering events in

the system in a self-consistent way.²⁴ Finally, the outgoing Auger electron is described by a time-reversed low-energy electron diffraction (LEED) state: $\phi_{\vec{k}, m_s}^{\text{final}} = T \phi_{-\vec{k}, -m_s}^{\text{LEED}}$, which is characterized by its wave vector \vec{k} and spin character m_s with the time-reversal operator $T = -i\sigma_y K$.²⁵ For the spin-polarized case one has²⁶

$$\begin{aligned} \phi_{\vec{k}, m_s}^{\text{LEED}}(\vec{r}_n, E) &= 4\pi \sqrt{\frac{E+c^2}{2E+c^2}} \sum_{\Lambda} i^l C_{\Lambda}^{m_s} Y_l^{\mu-m_s*}(\hat{k}) \\ &\times \sum_m e^{i\vec{k}\vec{R}_m} \sum_{\Lambda'} \tau_{\Lambda \Lambda'}^{nm}(E) Z_{\Lambda'}^n(\vec{r}_n, E), \quad (7) \end{aligned}$$

where the summation runs over the lattice sites m at positions \vec{R}_m .

Insertion of these ingredients into Eq. (1) leads after some simple transformations to the following general expression for the intensity of the spin- and angular-resolved Auger-electron current,

$$\begin{aligned} I^{m_s \propto} &\left(\frac{E_D + c^2}{2E_D + c^2} \right) \int dE_B \int dE_C \sum_{\substack{\Lambda \Lambda' \\ \Lambda'' \Lambda'''}} \mathfrak{T}_{\Lambda \Lambda'}^{nn}(E_C) \\ &\times \mathfrak{T}_{\Lambda'' \Lambda'''}^{nn}(E_B) \sum_{\substack{\Lambda_1 \Lambda_2 \\ \Lambda'_1 \Lambda'_2}} \sum_{m_1, m_2} \tau_{\Lambda'_1 \Lambda_1}^{nm_1}(E_D) \tau_{\Lambda'_2 \Lambda_2}^{nm_2*}(E_D) \\ &\times [i^{-l_1} C_{\Lambda_1}^{-m_s} Y_{l_1}^{\mu_1+m_s}(-\hat{k}) e^{i\vec{k}\vec{R}_{m_1}}]^* \\ &\times [i^{-l_2} C_{\Lambda_2}^{-m_s} Y_{l_2}^{\mu_2+m_s}(-\hat{k}) e^{i\vec{k}\vec{R}_{m_2}}] \\ &\times [M(\Lambda_A, \Lambda'_1, \Lambda, \Lambda'') - M(\Lambda_A, \Lambda'_1, \Lambda, \Lambda''')] \\ &\times [M(\Lambda_A, \Lambda'_2, \Lambda', \Lambda''') - M(\Lambda_A, \Lambda'_2, \Lambda''', \Lambda')]^*. \quad (8) \end{aligned}$$

Here we used the short notation

$$\begin{aligned} M(\Lambda_A, \Lambda_D, \Lambda_C, \Lambda_B) &= \sum_{l=|l_D-l_C|}^{(l_D+l_C)/2} \frac{4\pi}{2\Lambda+1} \\ &\times \left[\int r^2 dr g_{\Lambda_A} g_{\Lambda_B} \bar{R}_{\Lambda_D \Lambda_C} A_{\Lambda_B \Lambda_A}^l \right. \\ &\left. + \int r^2 dr f_{\Lambda_A} f_{\Lambda_B} \bar{R}_{\Lambda_D \Lambda_C} A_{-\Lambda_B - \Lambda_A}^l \right] \\ &\times \delta_{(\mu_A - \mu_B), -(\mu_D - \mu_C)} \quad (9) \end{aligned}$$

for the Coulomb matrix elements that are given explicitly in Refs. 11 and 16.

The expression given above allows one to deal with spin- and angle-resolved CVV AES and accounts for all multiple-scattering events for the final-state (Auger) electrons. A corresponding nonrelativistic formalism has been presented before by several authors.²⁷⁻²⁹ As it has been demonstrated by Idzerda and Ramaker²⁷ this enables one to describe and discuss low-energy (this means low kinetic energy of the Auger electrons) angle-resolved Auger spectra in a very satisfying way. Although angle-resolved AES can also be used to study

magnetic properties^{30,28} it has so far primarily been exploited to obtain structural informations. In the following the main concern is with magnetic properties and the role of spin-orbit coupling. For this reason the fully relativistic approach presented above is most appropriate. In addition, the case studied below corresponds to the high-energy AES situation. As a consequence, scattering for the final state can be ignored. The corresponding single scatterer approximation implies that the summations over sites m_1 and m_2 in Eq. (8) can be dropped and that the scattering path operator $\tau_{\Lambda\Lambda'}^{nm}$ can be replaced by the single-site t matrix $t_{\Lambda\Lambda'}^n$. If the Auger experiment is done in addition in an angle-integrated mode, the expression in Eq. (8) has to be averaged with respect to its \vec{k} dependence leading to

$$\begin{aligned}
I^{m_s\alpha} & \left(\frac{E_D + c^2}{2E_D + c^2} \right) \int dE_B \int dE_C \sum_{\substack{\Lambda\Lambda' \\ \Lambda''\Lambda'''}} \Im \tau_{\Lambda\Lambda'}^{nn}(E_C) \\
& \times \Im \tau_{\Lambda''\Lambda'''}^{nn}(E_B) \sum_{\substack{\Lambda_1\Lambda_2 \\ \Lambda'_1\Lambda'_2}} C_{\Lambda_1}^{m_s} C_{\Lambda_2}^{m_s} t_{\Lambda'_1\Lambda_1}^n(E_D) t_{\Lambda'_2\Lambda_2}^{n*}(E_D) \\
& \times [M(\Lambda_A, \Lambda'_1, \Lambda, \Lambda'') - M(\Lambda_A, \Lambda'_1, \Lambda, \Lambda'')] \\
& \times [M(\Lambda_A, \Lambda'_2, \Lambda', \Lambda''') - M(\Lambda_A, \Lambda'_2, \Lambda''', \Lambda')]*.
\end{aligned} \tag{10}$$

If one is dealing with a paramagnetic system the radial part of the Coulomb integral in Eq. (9) does not depend on the magnetic quantum numbers μ_i . Ignoring or averaging the μ dependence of the scattering path operator one can in this case further simplify the above expression by evaluating the sums over the magnetic quantum numbers analytically, as has been done by Szunyogh *et al.*¹¹ Identifying the imaginary part of the scattering path operator with the normalized κ -like density of states $n_\kappa(E)$ these authors could in particular demonstrate that the CVV AES intensity can be expressed by a cross-section-weighted self-convolution of the density of states for the occupied valence-band states (for further details see Ref. 11).

Because for magnetic solids the radial part of the various involved wave functions ψ , Z_Λ , and ϕ_{final} in Eqs. (8) and (10), respectively, depends also on the magnetic quantum number, the above-mentioned simplification for the paramagnetic case cannot be exploited. As a consequence, the expressions in Eqs. (8) and (10) have to be used for the angle-resolved and angle-integrated case, respectively. Nevertheless, as will be shown below, one can still interpret CVV AES spectra to represent essentially a self-convolution of density-of-states curves below the Fermi level.

Finally, it should be emphasized that an approach as sketched here presents a rather extreme point of view. First of all it assumes that the Auger (relaxation) step can be decoupled from the preparation (excitation) step. In addition it describes the Auger spectra on the basis of the electronic structure of the ground state alone. This implies, in particular, that the wave functions ψ , Z_Λ , and ϕ_{final} occurring in Eqs. (3), (6), and (7), respectively, are determined within a ground-state calculation. The limitations and problems of this point of view have been discussed among others by

Szunyogh *et al.*¹¹ A simple way to improve this approach is to account for the presence of the core hole explicitly when calculating the initial state for the Auger relaxation process. This means that the electronic structure of the system has to be calculated self-consistently with a core state of the excited atom being unoccupied. This situation corresponds to an impurity in an otherwise perfect host and can be dealt with either by the supercell technique³¹ or by using the Green's function formalism.³²

The formalism outlined above has been implemented by making use of the spin-polarized version of the Korriga-Kohn-Rostoker³³ (SPR-KKR) method making use of the atomic sphere approximation for the shape of the potential, the charge density, and the wave functions. All exchange and correlation effects have been treated within the framework of local spin density-functional theory (SDFT).²⁰ Using the SPR-KKR gives direct access to the electronic Green's function of the system. This has been exploited here to account for the presence of a core hole by performing corresponding impurity-type calculations for the underlying electronic structure. In principle it is also possible to account for surface effects, when using the SPR-KKR.³⁴ These can safely be ignored here because of the high kinetic energy of the emitted Auger electrons (about 330 eV in the case of the $M_{4,5}VV$ spectra and about 700 eV for the $L_{2,3}VV$ spectra of Fe; see below). In addition only pure elements will be dealt with in the following.

To allow for a direct comparison of the resulting theoretical spectra with experiment one has to account for various intrinsic and apparatusive broadening mechanisms in a proper way. To represent intrinsic lifetime effects Lorentzian broadening has been applied with an energy-dependent broadening parameter $\Gamma_L(\Delta E)$ (full width at half maximum) that increases quadratically with the energy difference $\Delta E = (E_F - E_B)$ and $(E_F - E_C)$, respectively, with E_F the Fermi energy. The finite apparatusive resolution has been represented by Gaussian broadening with the parameters Γ_G given below standing for the full width at half maximum.

III. RESULTS AND DISCUSSION

A. Application to paramagnetic solids

The expressions given in Eqs. (8) and (10) are quite general and can be applied straightforwardly to paramagnetic solids. In Fig. 1 the calculated $M_{4,5}VV$ AES spectrum of paramagnetic fcc Pd is shown (for the calculations for Pd the initial core hole in the $3d$ shell has been ignored—see Sec. II and the discussion below). Within the formalism presented above this spectrum emerges from a plain superposition of the partial M_4VV and M_5VV spectra that are shifted against one another by the spin-orbit splitting of the $3d$ core states (5.5 eV). Weighting the partial spectra with $\frac{1}{4}$ and $\frac{1}{6}$, respectively, according to the number of individual core states within the $3d_{3/2}$ and $3d_{5/2}$ shells and ignoring their spin-orbit splitting does not lead to full coincidence of the partial M_4VV and M_5VV spectra. In particular, one finds the M_5VV to have a lower maximum amplitude and full width at half maximum and to be more asymmetric than the M_4VV spectrum. This is a clear consequence of the inclusion of the spin-orbit coupling for the valence-band states.

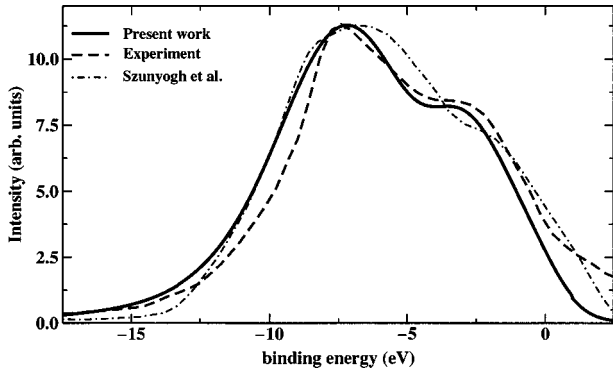
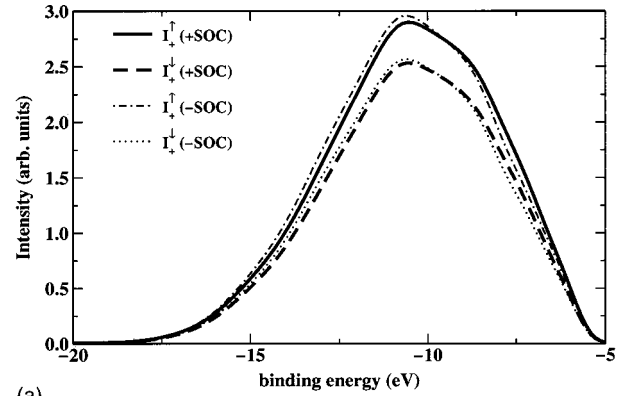


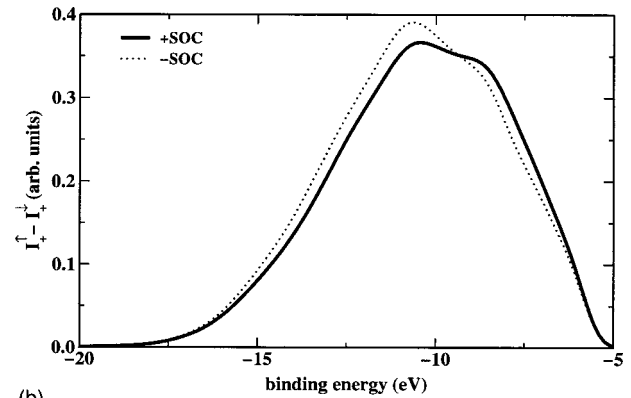
FIG. 1. Spin- and angle-integrated $M_{4,5}VV$ AES spectrum of paramagnetic Pd. The experimental spectrum has been recorded by Weightman and Andrews (Ref. 40). The second theoretical spectrum stems from Szunyogh and co-workers (Ref. 11).

To allow the comparison with experiment, the partial M_4VV and M_5VV spectra have been broadened in an appropriate way using $\Gamma_L(\Delta E) = (0.4 + 0.03\Delta E^2)$ eV and $\Gamma_G = 1.65$ eV. To compare the theoretical and experimental spectra both have been scaled to agree with respect to their maximum. In addition, one has to mention that the energy zero in Fig. 1 corresponds to the threshold of the theoretical M_4VV spectrum. This energy scale is connected to the kinetic energy recorded in experiment via the corresponding binding energy of the core electrons. Because binding energies calculated within SDFT deviate normally some few percent from experimental values, the experimental Auger spectrum has been aligned with the theoretical one for comparison. As can be seen in Fig. 1, a rather satisfying agreement is achieved with experiment this way. This means that the straightforward superposition of the partial M_4VV and M_5VV spectra is well justified. As a consequence, one can conclude that there are no strong Coster-Kronig Auger processes that affect the ratio of these partial spectra (see below). Comparing the theoretical spectrum with that obtained by Szunyogh *et al.*¹¹ one finds some slight differences. These may be ascribed to the approximation with respect to the μ dependence of $\tau_{\Lambda\Lambda}^{nn}$, used by these authors to simplify the expression given in Eq. (10). On the basis of the results given below, however, it seems to be more likely that the differences are due to details in the potential construction and/or the broadening applied. It should be added here that an alternative approach to deal with the $M_{4,5}VV$ spectrum of Pd based on intermediate-coupling theory has been used by Cini and Verdozzi.³⁵

The experimental spectrum shown in Fig. 1 has been obtained using unpolarized x-rays from a Cu anode for the initial excitation step, i.e., for the creation of the electron hole in the $M_{4,5}$ shell. Using circularly polarized radiation instead would lead to a preferential occupation of the various sublevels of the M_4 and M_5 shells that differ with respect to the magnetic quantum number μ . As could be demonstrated by Stoppmanns *et al.*⁵ for various alkali metals, this leads to a spin-polarized Auger-electron current even for paramagnetic solids. A corresponding theoretical description of this type of experiment has been given by Yuan *et al.*¹² However, these authors accounted in their calculations only for the spin-orbit coupling with respect to the involved core levels.



(a)



(b)

FIG. 2. Spin-resolved M_5VV AES spectra for paramagnetic Pd calculated assuming excitation using right circularly polarized light. The curves marked +SOC and -SOC have been obtained by including and suppressing, respectively, the spin-orbit coupling for the valence-band and time-reversed LEED states. Bottom: corresponding difference spectra $\Delta I = I^\uparrow(\pm \text{SOC}) - I^\downarrow(\pm \text{SOC})$.

In contrast to this approach, the present formalism includes the spin-orbit coupling for all initial as well as final states. To investigate the importance of this extension the spin-resolved M_5VV Auger spectra of Pd have been calculated in two different ways. The first set of calculations has been done by applying the fully relativistic formalism as it has been outlined above. For the second set of calculations the spin-orbit coupling has been suppressed for the valence band and time-reversed LEED states when solving the Dirac equation.³⁶ In both cases it has been assumed that the preparation step is done by exciting only M_5 core electrons to states just above the Fermi level using right circularly polarized radiation. The corresponding theoretical x-ray absorption cross section has been calculated in a fully relativistic way as described in Ref. 37. As can be seen in the top panel of Fig. 2, both sets of calculations lead to a substantial spin-polarization for the Auger electrons. In addition, one notes some deviations of corresponding spin-projected Auger spectra from one another, which leads for the difference spectra $\Delta I = I^\uparrow(\pm \text{SOC}) - I^\downarrow(\pm \text{SOC})$ (see lower panel of Fig. 2) to rather different line shapes. While there is a clear and prominent peak for the difference spectrum $\Delta I = I^\uparrow(-\text{SOC}) - I^\downarrow(-\text{SOC})$ if spin-orbit coupling is suppressed (-SOC), ΔI has a rather flat top if the spin-orbit coupling is included (+SOC).

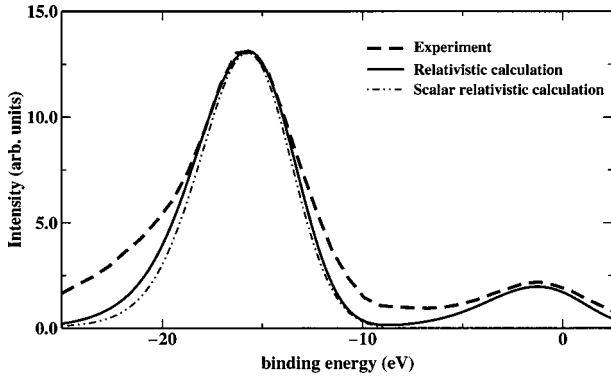
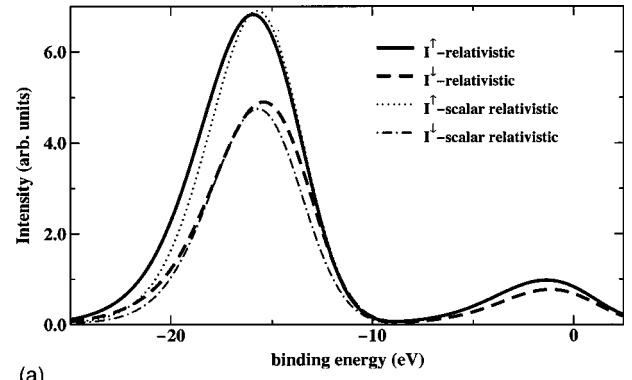


FIG. 3. Spin- and angle-integrated $L_{2,3}VV$ AES of ferromagnetic Fe calculated using the expression in Eq. (10). The corresponding experimental data stem from Sarma *et al.* (Ref. 38). Results of scalar relativistic calculations have been added and aligned with the partial L_3VV spectrum.

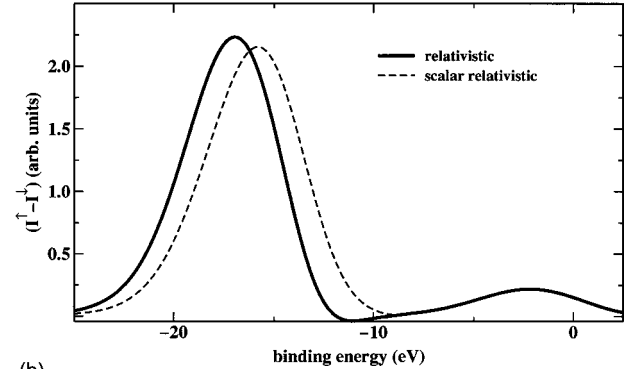
B. Application to ferromagnetic solids

In Fig. 3 the results of calculations of the $L_{2,3}VV$ spin- and angle-integrated Auger spectrum of ferromagnetic bcc Fe is shown. As for the case of Pd, the spectra shown here have been obtained by ignoring the initial core hole in the $2p$ shell (see below). Again, an appropriate broadening has been applied using $\Gamma_L(\Delta E) = (0.4 + 0.01\Delta E^2)$ eV and $\Gamma_G = 1.88$ eV to allow one a direct comparison with experiment. Concerning the shape and width of the partial L_2VV and L_3VV spectra a rather good agreement with the experimental spectrum recorded by Sarma *et al.*³⁸ is achieved. Also the spin-orbit splitting of the $2p$ levels (12.5 eV) is in satisfying agreement with experiment. Because of this relatively large splitting the partial L_2VV and L_3VV spectra hardly overlap. Concerning the intensity of the experimental partial spectra one notes that their ratio is far from the ideal ratio 4:2 that is expected from the number of sublevels in the $2p_{3/2}$ and $2p_{1/2}$ shells. This behavior is ascribed to a strong Coster-Kronig $L_2L_3M_{4,5}$ decay channel that is in competition with the L_2VV transitions.^{39,38} According to this, it is well justified to scale down the intensity of the theoretical partial L_2VV spectrum to agree with the experimental one with respect to its maximum amplitude.

Theoretical spin-resolved $L_{2,3}VV$ Auger spectra for ferromagnetic bcc Fe are shown in Fig. 4. The partial L_2VV spectrum has been normalized using the same scaling factor as used above. For the calculation of the theoretical spectra excitation with unpolarized radiation has been assumed. As a consequence, the spin polarization of the Auger electrons is primarily due to the intrinsic exchange splitting. As one can see in Fig. 4, the partial majority-spin spectrum I^\uparrow is about 0.3 eV broader than the minority-spin spectrum I^\downarrow and shifted by about 0.5 eV towards lower energy. The resulting difference spectrum $(I^\uparrow - I^\downarrow)$ has its maximum at about 1.2 eV lower energy than the total spectrum $(I^\uparrow + I^\downarrow)$. The relative spin polarization $P = (I^\uparrow - I^\downarrow)/(I^\uparrow + I^\downarrow)$ depends slightly on the broadening applied. Nevertheless, its maximum value ($\approx 30\%$) agrees very well with that given by Landolt and Mauri³ and Landolt.³⁹ Unfortunately, a more detailed comparison with the experimental work of these authors is not possible because they give only the relative spin polarization P , for which the choice of the background introduces some



(a)



(b)

FIG. 4. Top: Spin-resolved $L_{2,3}VV$ AES $I^{l(\downarrow)}$ of ferromagnetic bcc Fe calculated using the expression in Eq. (10). Bottom: The corresponding difference spectrum $(I^\uparrow - I^\downarrow)$. Results of scalar relativistic calculations have been added and aligned with the partial L_3VV spectrum.

ambiguity of the absolute value within a factor of ≈ 1.3 .³⁹ While Landolt and co-workers used unpolarized electrons for the excitation step, Sinković *et al.* used linearly polarized x-rays⁶ with the photon energy adjusted to the L_3 -absorption edge ($\hbar\omega = 707$ eV, on-resonant) and far above it ($\hbar\omega = 820$ eV, off-resonant). For the off-resonant situation one can ignore the exchange splitting for the final states of the excitation process. As a consequence one has only a slight preferential depopulation of the various sublevels of the $2p_{3/2}$ shell due to the use of linearly polarized radiation and the small exchange splitting of the initial states. According to this one may expect that the resulting spin-resolved Auger spectrum primarily reflects the exchange splitting in the valence band. This could be demonstrated by Sinković *et al.*⁶ by comparing the self-convoluted density-of-states curves (DOS) for the majority and minority spin electrons, respectively, to their experimental spectra. While this approach led for the off-resonant situation to a rather reasonable agreement of the convoluted DOS curves with the spin-resolved Auger spectra, it was found for the on-resonant situation that the amplitude of the experimental minority partial spectrum is reduced in an appreciable way. This finding was ascribed to the nonzero spin polarization P_{core} of the initial hole together with a difference in the spin-dependent Auger matrix elements $M_{\uparrow\uparrow}(=M_{\downarrow\downarrow})$ and $M_{\uparrow\downarrow}(=M_{\downarrow\uparrow})$. The model based on these parameters led to results in rather good agreement with experiment for the ratio $M_{\uparrow\uparrow}/M_{\uparrow\downarrow} \sim 2/3$ (for further details see Ref. 6). Calculating the energy- and polarization- (λ) dependent x-ray absorption coefficient $\mu_\lambda(\hbar\omega)$,³⁷ as it is

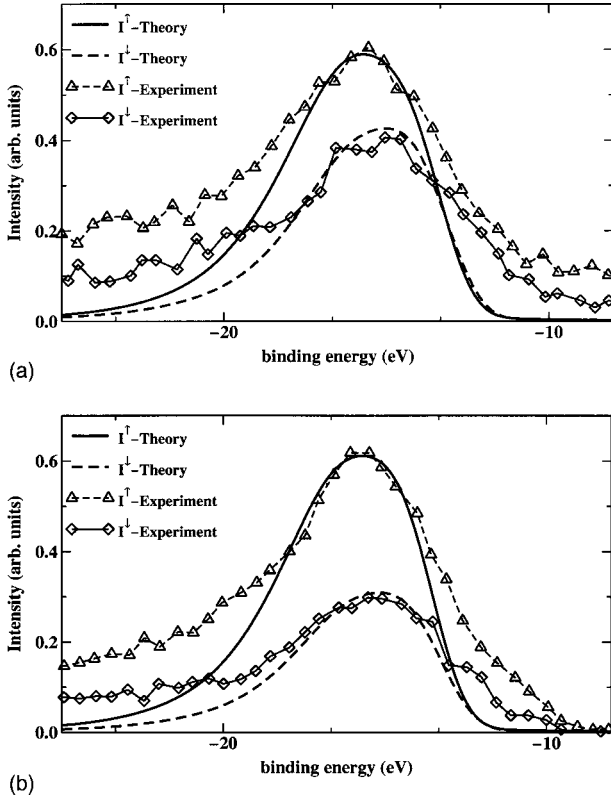


FIG. 5. Top: Spin-resolved L_3VV AES spectra for ferromagnetic bcc Fe using off-resonant excitation with linear polarized light. Bottom: as in the top except using on-resonant excitation. Experimental spectra have been recorded by Sinković *et al.* (Ref. 6).

done here, the spin polarization P_{core} of the core states is automatically accounted for. The description of the Auger process presented above, in particular the matrix elements given in Eq. (9), account for all spin-dependent processes represented by the effective matrix elements $M_{\uparrow\uparrow}$ and $M_{\uparrow\downarrow}$. This is demonstrated in Fig. 5 where corresponding spectra are compared with the experimental data of Sinković *et al.* As done in the case of the $M_{4,5}VV$ spectra of Pd the experimental spectra have been scaled and shifted in energy to allow comparison with theory. However, it has to be emphasized that the same energy shift and scaling has been applied. In particular the ratio of the majority and minority spectra were not changed. In agreement with experiment, it is found that the majority-spin spectra for the on- and off-resonance situations are somewhat broader and shifted by 0.5 eV to lower energies with respect to the corresponding minority-spin spectra. In the energy range from about -9 eV to -14 eV shown in Fig. 5 the experimental spectra have some photoemission contributions stemming from the valence-band states.⁶ Taking this into account there is a rather good agreement of theory and experiment with respect to the shape and width of the various spectra. Most important, however, is that the calculations properly account for the increase of the spin polarization at the maximum when going from the off-resonant ($P=0.21$) to the on-resonant ($P=0.37$) situation without use of any adjustable parameters.

In addition to the calculations that ignored the initial core hole a second set of calculations were done taking into account the core hole for the initial state (see Sec. II) in the potential construction. This means that an impurity-type cal-

ulation has been done for the central atom that undergoes the Auger transition. The resulting spin-resolved $L_{2,3}VV$ spectra differ only slightly from the results given in Figs. 3 and 4. The most prominent consequence of the inclusion of the core hole is that the maximum spin polarization P is reduced to about 0.27.

Because of the quite complex nature of the wave functions in Eqs. (3) and (7) a simple analysis of the theoretical spectra in Figs. 3 and 4 is not possible. However, to allow one a more detailed discussion, an additional scalar relativistic calculation of the spin-resolved L_3VV Auger spectrum of bcc Fe has been performed, neglecting the spin-orbit coupling for all involved electronic states. Within this framework the corresponding spin-dependent AES intensity $I^{m_s}(E)$ is given by a weighted self-convolution of the DOS below the Fermi level

$$I^{m_s}(E) = \int_{E+E_{\Lambda_A}-E_F}^{E_F} dE' \times \sum_{l,l',m'_s} n_{lm_s}(E') n_{l'm'_s}(E'') W_{lm_s,l'm'_s}(E',E''), \quad (11)$$

where E is the energy of the outgoing electron, E_{Λ_A} is the energy of the involved core level, E_F is the Fermi energy, and the restriction $E-E'=E''-E_{\Lambda_A}$ applies due to the energy conservation. Furthermore, $n_{lm_s}(E)$ is the angular-momentum- and spin-resolved DOS while $W_{lm_s,l'm'_s}(E,E')$ is an effective cross section combining the various angular matrix elements as well as the radial Coulomb matrix elements (for further details see Ref. 16). The corresponding spin-integrated spectrum has been added in Fig. 3. For this purpose, it has been scaled to agree with the maximum of the partial L_3VV spectrum and shifted in energy to have the same threshold at -15.7 eV binding energy. As can be seen, these two spectra differ slightly in shape. Most important, the width of the scalar relativistic spectrum measured at half maximum is about 1 eV smaller than that of its fully relativistic counterpart. This has to be ascribed to the influence of the spin-orbit coupling of the 3d electrons (about 0.2 eV in average) on the valence-band states. An additional source for the difference is the exchange splitting of the core levels that has been neglected for the scalar relativistic calculations. For the $2p_{3/2}$ shell of bcc Fe the various sublevels labeled with the magnetic quantum number μ are spread over a range of 1 eV. In Fig. 4 (top) one can see that the spin-resolved scalar relativistic spectra for the majority and minority spin character have a slightly different energy shift and change in amplitude with respect to their fully relativistic counterparts. As a consequence, the maxima of the I^\uparrow and I^\downarrow spectra calculated in a scalar relativistic way nearly coincide. The relativistic spectra, on the other hand, are shifted apart by about 0.5 eV as is found in experiment (see above). As a consequence of the various differences to be noted in Fig. 4 the position of the maximum in the experimental polarization curve P is also better reproduced by the relativistic calculations than by the scalar relativistic ones.

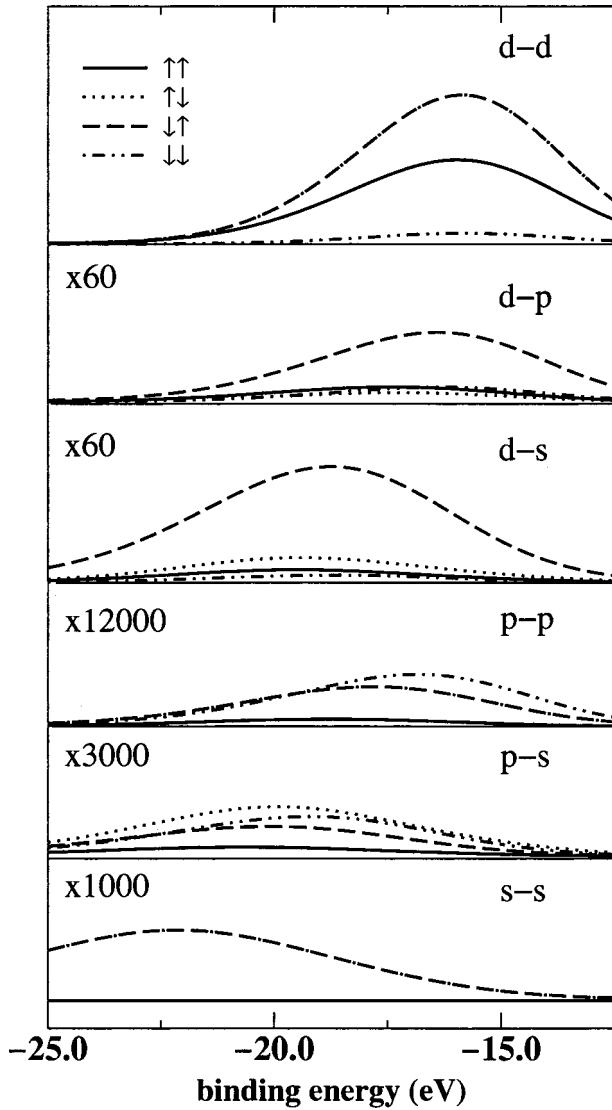


FIG. 6. Spin- and angular-momentum-resolved L_3VV AES spectrum calculated in a scalar relativistic way using the expression given in Eq. (11).

In spite of the pronounced influence of the spin-orbit coupling in the case of Fe and the better agreement with experiment found for the relativistic than for the scalar relativistic calculations, the latter ones are nevertheless very helpful for a more detailed analysis of the rather complex CVV Auger spectra. In particular, it is straightforward to decompose the spin-resolved spectra according to the angular-momentum character of the valence-band states involved within the scalar relativistic approach [see Eq. (11)]. From Fig. 6, which shows the corresponding curves for bcc Fe, it is obvious that the $d-d$ contributions are by far dominating. All other contributions are at least by a factor of 50 smaller. This behavior is very similar to that found for the SR-APS spectrum of bcc Fe.¹⁶ Of course this has to be ascribed to some extent to the high d -like density of states. More important, however, is the weighting introduced by the Coulomb matrix elements that strongly favor the $3d$ electrons because these have an overlap with the $2p$ -core wave functions higher than the more spreadout $4s$ and $4p$ electrons. For some of the dominant d contributions the effective cross sections $W_{lm_s, l'm'_s}(E, E')$

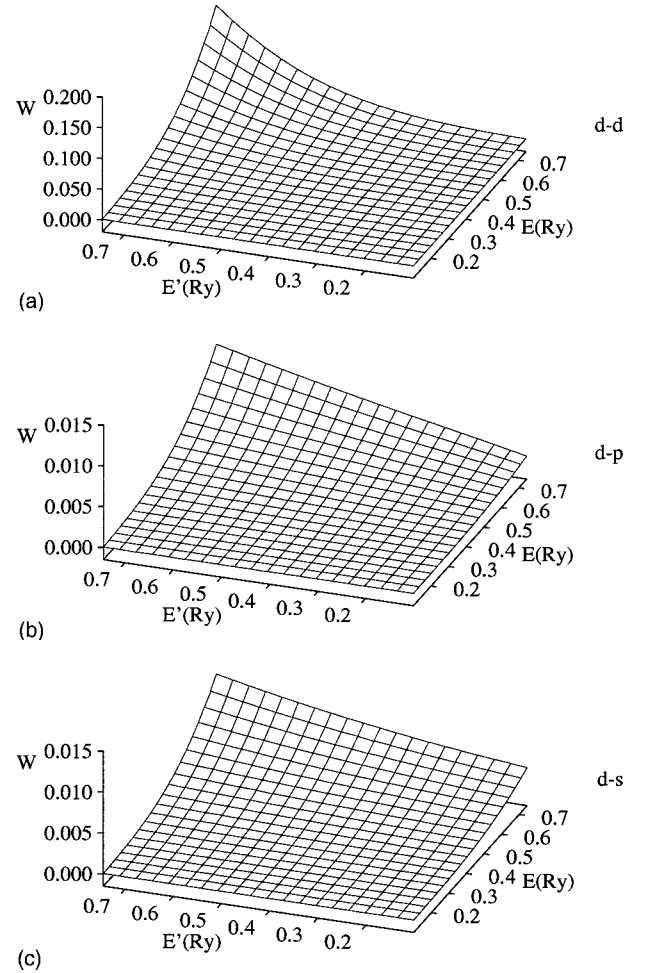


FIG. 7. Selected spin- and angular-momentum-resolved cross sections $W_{lm_s, l'm'_s}(E, E')$ [see Eq. (11)] for bcc Fe corresponding to Fig. 6, i.e., for $l=d, l'=s, p, d$, and $m_s=m'_s=\uparrow$. The upper energy limit 0.745 Ry for E and E' corresponds to the Fermi energy.

are shown in Fig. 7. These functions depend only slightly on the spin quantum numbers m_s and m'_s . For that reason only data for $m_s=m'_s=\uparrow$, i.e., the majority spin direction, are shown. In line with the decomposition made in Fig. 6, one notices that the $d-d$ cross sections are about an order of magnitude larger than the other ones. In addition, one can see that there is a rather pronounced energy dependence for $W_{lm_s, l'm'_s}(E, E')$ which is strongest for transitions that involve states in the vicinity of the Fermi energy.

IV. SUMMARY

A fully relativistic description for the spin-resolved CVV AES has been presented that is applicable to paramagnetic as well as to ferromagnetic solids. The most prominent feature of this approach is that it treats all possible sources for the spin polarization of Auger electrons on the same level. This also applies to the treatment of the initial preparation step if this is done by using polarized x-ray radiation. The wide applicability of our approach has been demonstrated by the results of calculations of the $M_{4,5}VV$ AES spectra of Pd and the $L_{2,3}VV$ AES spectra of Fe. In both cases, the importance

of the spin-orbit coupling not only for the core states but also for the valence states was emphasized. This could be demonstrated by accompanying calculations for which the spin-orbit coupling was partially or completely suppressed. This auxiliary calculations allowed one, in addition, a detailed analysis of the various spin- and angular-momentum-resolved cross sections.

ACKNOWLEDGMENTS

This work was supported by the German ministry for education and research (BMBF) under Contract No. 05 SC8WMA 7 within the program *Zirkular polarisierte Synchrotronstrahlung: Dichroismus, Magnetismus und Spinorientierung*.

-
- ¹ *Core Level Spectroscopies for Magnetic Phenomena: Theory and Experiment*, edited by P.S. Bagus, G. Pacchioni, and F. Parmigiani (Plenum, New York, 1995).
- ² *Spin-Orbit Influenced Spectroscopies of Magnetic Solids*, edited by H. Ebert and G. Schütz, Lecture Notes in Physics Vol. 466 (Springer-Verlag, Heidelberg, 1996).
- ³ M. Landolt and D. Mauri, Phys. Rev. Lett. **49**, 1783 (1982).
- ⁴ R. Allenspach, D. Mauri, M. Taborelli, and M. Landolt, Phys. Rev. B **35**, 4801 (1987).
- ⁵ P. Stoppmanns *et al.*, J. Phys.: Condens. Matter **6**, 4225 (1994).
- ⁶ B. Sinković, E. Shekel, and S.L. Hulbert, Phys. Rev. B **52**, R15 703 (1995).
- ⁷ W. Kuch *et al.* (unpublished).
- ⁸ W. Nolting, G. Geipel, and K. Ertl, Phys. Rev. B **45**, 5790 (1992).
- ⁹ M. Potthoff, J. Braun, G. Borstel, and W. Nolting, Phys. Rev. B **47**, 12 480 (1993).
- ¹⁰ M. Cini, Phys. Scr. **T41**, 59 (1992).
- ¹¹ L. Szunyogh, P. Weinberger, and J. Redinger, Phys. Rev. B **46**, 2015 (1992).
- ¹² J. Yuan, L. Fritsche, and J. Noffke, Phys. Rev. B **56**, 9942 (1997).
- ¹³ J.J. Lander, Phys. Rev. **91**, 1382 (1953).
- ¹⁴ B. Sinković *et al.*, Phys. Rev. Lett. **62**, 2740 (1989).
- ¹⁵ B. Sinković *et al.*, Phys. Rev. B **52**, R6955 (1995).
- ¹⁶ H. Ebert and V. Popescu, Phys. Rev. B **56**, 12 884 (1997).
- ¹⁷ V. Popescu *et al.*, Phys. Rev. B **61**, 15 241 (2000).
- ¹⁸ D. Chattarji, *The Theory of Auger Transitions* (Academic Press, London, 1976).
- ¹⁹ H. Ebert, J. Phys.: Condens. Matter **1**, 9111 (1989).
- ²⁰ A.H. MacDonald and S.H. Vosko, J. Phys. C **12**, 2977 (1979).
- ²¹ M.E. Rose, *Relativistic Electron Theory* (Wiley, New York, 1961).
- ²² E. Tamura, Phys. Rev. B **45**, 3271 (1992).
- ²³ T. Huhne *et al.*, Phys. Rev. B **58**, 10 236 (1998).
- ²⁴ B.L. Gyorffy and M.J. Stott, in *Band Structure Spectroscopy of Metals and Alloys*, edited by D.J. Fabian and L.M. Watson (Academic Press, New York, 1973), p. 385.
- ²⁵ B. Ackermann and R. Feder, Solid State Commun. **54**, 1077 (1985).
- ²⁶ H. Ebert and G.Y. Guo, J. Magn. Magn. Mater. **148**, 174 (1995).
- ²⁷ Y.U. Idzerda and D.E. Ramaker, Phys. Rev. Lett. **69**, 1943 (1992).
- ²⁸ P. Rennert, Y. Kucherenko, and L. Niebergall, J. Electron Spectrosc. Relat. Phenom. **93**, 239 (1998).
- ²⁹ G. Hörmandinger, P.W. Weinberger, and J. Redinger, Phys. Rev. B **40**, 7989 (1989).
- ³⁰ D.E. Ramaker, R.A. Fry, and Y.U. Idzerda, J. Electron Spectrosc. Relat. Phenom. **72**, 169 (1995).
- ³¹ M. Alouani, Phys. Rev. B **49**, 16 038 (1994).
- ³² R. Zeller, Z. Phys. B: Condens. Matter **72**, 79 (1988).
- ³³ H. Ebert, in *Electronic Structure and Physical Properties of Solids*, edited by H. Dreyssé, Lecture Notes in Physics Vol. 535 (Springer, Berlin, 2000), p. 191.
- ³⁴ Újfalussy, L. Szunyogh, and P. Weinberger, in *Properties of Complex Inorganic Solids*, edited by A. Gonis, A. Meike, and P.E.A. Turchi (Plenum Press, New York, 1997), p. 181.
- ³⁵ M. Cini and C. Verdozzi, J. Phys.: Condens. Matter **1**, 7457 (1989).
- ³⁶ H. Ebert, H. Freyer, A. Vernes, and G.-Y. Guo, Phys. Rev. B **53**, 7721 (1996).
- ³⁷ H. Ebert, Rep. Prog. Phys. **59**, 1665 (1996).
- ³⁸ D.D. Sarma *et al.*, Phys. Rev. B **48**, 6822 (1993).
- ³⁹ A. Landolt, in *Polarized Electrons in Surface Physics*, edited by R. Feder (World Scientific Publishing, Singapore, 1985), p. 387.
- ⁴⁰ P. Weightman and P.T. Andrews, J. Phys. C **13**, L815 (1980).